J.-M. Biannic, C. Roos, J. Lesprier
(ONERA)

E-mail: jean-marc.biannic@onera.fr

DOI: 10.12762/2017.AL13-02

Nonlinear Structured H_∞ Controllers for Parameter-Dependent Uncertain Systems with Application to Aircraft Landing

A new design methodology inspired by dynamic inversion techniques is proposed in this paper. It combines partially linearizing inner-loops with structured and robust outer-loops, which are designed using a non-smooth multi-model H_∞ optimization approach. The proposed methodology also includes a robustness analysis scheme providing worst-case configurations, which are then used to enrich the bank of design models and thus iteratively improve the robustness properties of the designed outer-loops. Our approach is successfully tested on a realistic nonlinear aircraft control problem subject to large parametric variations and uncertainties.

Introduction

Robust feedback linearization techniques [10] have proved their efficiency in many aerospace applications, especially to control highly maneuverable aircraft or UAVs in large operating domains [25, 2, 20, 21, 11, 4]. Interestingly, such techniques do not only permit a large class of nonlinear systems to be linearized and decoupled, but also make it possible to adapt the control laws to the operating point. Thus, they become a competitive alternative to standard gain-scheduling techniques, which often entail many adjustments, or to LPV control design strategies, which require high fidelity LPV models [15]. However, standard dynamic inversion methods are often criticized for their lack of robustness and the need for an accurate model. This drawback is generally bypassed via robust linear outer-loops [6], which still require difficult and possibly time-consuming robustness evaluation *a posteriori* [18, 19]. Severe problems are also likely to occur when the actuator dynamics and limitations prevent an exact cancellation of the nonlinear terms. As emphasized in [12], it is therefore essential to take these dynamics into account in the design process. As observed in [8], one of the main reasons why standard dynamic inversion schemes exhibit poor robustness properties is due to the fact that the linearizing inner-loops are designed to convert the nonlinear system into a generic Brunovsky's form. Following an intuitive path, it is then proposed in [8] to design the inner-loops so that, for given operating conditions, the nonlinear system will converge to its Jacobian linearization. Hence, the design of the linear robust outer-loops is no longer based on a generic model, but now explicitly depends on the linearized dynamics of the initial plant. A similar path, consisting of promoting interactions between inner and outer loops, is followed in this paper. More precisely, as in [8] a feedback linearization step is applied so that, in some enlarged neighborhood of given trim conditions, the nonlinear plant behaves like its linearization. In a second step, a robust linear outer-loop is designed. The originality of our approach lies in the particular structure of our H_∞-based outer controller, which uses a nonlinear input as a key input to further enlarge the operating domain of the nonlinear closed-loop system. Various uncertainties are also taken into account in our procedure by a μ-based robustness analysis phase, during which worst-case configurations are identified and then used in an iterative multi-objective and multi-model H_∞ design process. It should be pointed out here that the resolution of such highly non-convex optimization problems has considerably improved in the past few years with recent advances in non-smooth H_∞ optimization algorithms [3, 9]. Indeed, the latter now make it possible to fix the order of the H_∞ controller as well as its structure and to consider multi-channel objectives and multiple models simultaneously, in order to increase the robustness margins. Such algorithms will then be a key ingredient in our proposed methodology.

The paper is organized as follows. A thorough description of the proposed methodology with its three main steps is first given. An application to a realistic landing aircraft control problem is then detailed. More precisely, we focuse on the longitudinal part and give many details on how the method is applied. Then we briefly deal with the lateral part of the control problem, before presenting the global landing application on the full nonlinear aircraft model using the designed controller. Finally, we conclude the paper.

Description of the methodology

Robust Nonlinear Compensation Technique

Consider a continuous-time parameter-dependent nonlinear input-affine system described as follows

$$\begin{cases} \dot{\xi}(t) &= f\left(\xi(t),\theta_p(t)\right)+G\left(\xi(t),\theta_p(t)\right)u(t) \\ u(t) &= L_A\left(u_c(t)\right) \end{cases} \quad (1)$$

where $\xi(t)\in\mathbb{R}^n$ denotes the physical states evolving in the admissible operating domain $\mathcal{X}\subset\mathbb{R}^n$. The realized control inputs $u(t)\in\mathbb{R}^m$ are derived from the commanded inputs $u_c(t)\in\mathbb{R}^m$ via linear time-invariant actuators – denoted by $L_A(.)$ – with unitary static gains. The nonlinearities and parametric variations of the system are captured by $f(.,.)\in\mathbb{R}^n$ and $G(.,.)\in\mathbb{R}^{n\times m}$, which both nonlinearly depend not only on the state vector but also on a set of parameters $\theta_p(t)\in\Theta\subset\mathbb{R}^r$.

Notation 1
Let us denote $\left(\bar{\xi},\bar{\theta}_p,\bar{u}\right)\in\mathbb{R}^n\times\mathbb{R}^r\times\mathbb{R}^m$ *an equilibrium point for system (1), thus satisfying:*

$$f\left(\bar{\xi},\bar{\theta}_p\right)+G\left(\bar{\xi},\bar{\theta}_p\right)\bar{u}=\bar{f}+\bar{G}\bar{u}=0 \quad (2)$$

and rewrite $f\left(\xi(t),\theta_p(t)\right)$ as follows:

$$f\left(\xi(t),\theta_p(t)\right)=\bar{f}+Ax(t)+\Delta_f(t) \quad (3)$$

where:

$$A=\left.\frac{\partial f}{\partial\xi}\right|_{\bar{\xi},\bar{\theta}_p} \quad \text{and} \quad x(t)=\xi(t)-\bar{\xi}(t) \quad (4)$$

and where $\Delta_f(t)$ denotes the deviation between the nonlinear function $f(.,.)$ and its linear approximation.

Assumption 1
There exists a constant matrix $B\in\mathbb{R}^{n\times m}$ *such that, for all* $\left(\xi(t),\theta_p(t)\right)\in\mathcal{X}\times\Theta$, *a* ***nonsingular*** *matrix* $\Lambda\in\mathbb{R}^{m\times m}$ *and a residual error matrix* $\Delta_G\in\mathbb{R}^{n\times m}$ *can be found such that:*

$$G\left(\xi(t),\theta_p(t)\right)=B\Lambda+\Delta_G \quad (5)$$

$$\forall\upsilon(t)\in\mathbb{R}^m,\ L_A\left(\Lambda^{-1}\upsilon(t)\right)\approx\Lambda^{-1}L_A\left(\upsilon(t)\right) \quad (6)$$

The square matrix Λ typically represents the control input efficiency. When considering aerospace systems evolving in standard operating domains, the above non-singularity assumption – connected to the notion of controllability – is not restrictive. Moreover, the variations of this diagonal-dominant matrix are mainly induced by slowly-varying terms, such as the dynamic pressure. This observation justifies the commutative property (6) between Λ^{-1} and the fast dynamics $L_A(.)$ of the actuators. Yet, a possible relaxation of (6) is introduced next.

Given any two signals $v(t)\in\mathbb{R}^m$ and $\zeta(t)\in\mathbb{R}^m$, let us now define the intermediate, input linearizing, control law

$$u_c(t)=\Lambda\left(\xi(t),\theta_p(t)\right)^{-1}\left(v(t)-\zeta(t)\right)+\bar{u} \quad (7)$$

Combining equations (7) and (1), one readily obtains with the above notation in mind:

$$\dot{x}=Ax+BL_A(v)+w_f+w_u \quad (8)$$

where:

$$w_f=\Delta_f-BL_A(\zeta) \quad (9)$$

$$w_u=(G-\bar{G})\bar{u}+\Delta_G\Lambda^{-1}L_A(v-\zeta) \quad (10)$$

As is clear from Equation (8), where parametric-dependence and time-dependence have been omitted to alleviate notation, the parameter-dependent nonlinear system (1) has been reduced to a linear model with a new control input v and two measured perturbations w_f and w_u. As is usual in dynamic inversion schemes, w_f can be partly canceled by an optimal choice of the auxiliary input signal $\zeta(t)$:

$$\hat{\zeta}(t)=Arg\min_{\zeta(t)\in\mathbb{R}^m}\left\|\Delta_f(t)-BL_A\left(\zeta(t)\right)\right\| \quad (11)$$

Remark 1
In the special case of square systems with idealized actuators (i.e., $L_A(u(t))=u(t)$*), one easily obtains* $w_f=0$ *with* $\hat{\zeta}(t)=B^{-1}\Delta_f(t)$.

Let us denote by $w=w_f+w_u$ the vector of remaining input perturbations, which cannot be canceled, and assume that the latter is available for feedback, via estimation, at least on a limited bandwidth. The following structure for the linear outer-loop may thus be considered:

$$v=K(s)\begin{pmatrix}\hat{w}\\ w_c\\ y\end{pmatrix} \quad (12)$$

where $\hat{w}$, w_c and y denote respectively the estimation of w, the target on the variables z to be tracked and the measurement signal. Without any significant loss of generality in most applications, both $y(t)=Cx(t)\in\mathbb{R}^p$ and $z(t)=Lx(t)\in\mathbb{R}^q$ are assumed to depend linearly on the state vector. The output feedback gain $K(s)$ in (12) is to be designed so as to satisfy the following requirements:

- good tracking properties, by minimizing the error between z and the reference signal $z_r=R(s)w_c$, where the LTI model $R(s)$ describes the nominal reference closed-loop dynamics,
- a reasonable control activity, which is indirectly obtained by limiting v to avoid control input saturations,
- good rejection of the perturbations $w=w_u+w_f$ that could not be entirely removed by the linearizing inner loop to enlarge the operating domain.

Denoting by $\Sigma_A(s)$ the transfer matrix associated to the linear operator $L_A(.)$ and by $\Sigma(s)$ the linearized plant interconnection:

$$\Sigma(s)=\begin{bmatrix}L\\ C\end{bmatrix}(sI-A)^{-1}\begin{bmatrix}I & B\end{bmatrix} \quad (13)$$

the above outer-loop design issue can be recast into a linear framework as a multi-objective H_∞ minimization problem. More precisely,

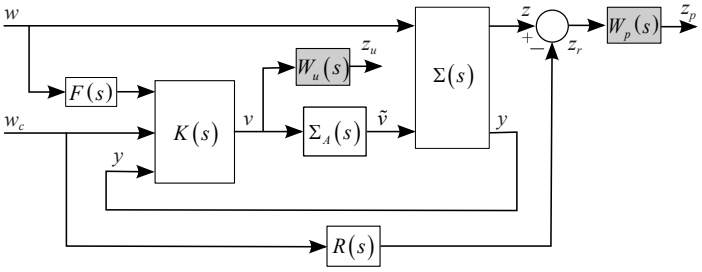

Figure 1 – H_∞ design-oriented scheme.

considering the linear interconnection of Figure 1, it is proposed to compute $K(s)$ as follows:

$$\hat{K}(s) = \underset{K(s)\in\mathcal{K}}{argmin} \left\| \mathcal{T}_{w_c \to z_p}(s) \right\|_\infty \tag{14}$$

with:

$$\begin{cases} \left\| \mathcal{T}_{w_c \to z_u}(s) \right\|_\infty \le \gamma_u \\ \left\| \mathcal{T}_{w \to z_p}(s) \right\|_\infty \le \gamma_r \end{cases} \tag{15}$$

The H_∞-norm minimization considered in (14) corresponds to the nominal tracking requirement. As is standard in H_∞ design approaches, a weighting function – typically a low-pass filter – $W_p(s)$ is introduced to specify the frequency domain where the tracking performance should be more efficient. Next, the second and third requirements are respectively taken into account by the additional two constraints in (15). The first one involves a high-pass weighting function $W_u(s)$ to minimize the control activity in the high-frequency domain. Finally, note the presence of a low-pass function denoted by $F(s)$, which can be viewed as an approximation of the estimation process ($\hat{w} \approx F(s)w$).

Problem (14)-(15) is a difficult non-convex and non-smooth optimization problem. However, it is now efficiently solved thanks to recent advances in non-smooth optimization techniques [3, 9]. Moreover, the structure of the controller as well as its order can also be fixed *a priori*, which makes the implementation easier. Last but not least, multiple models can be considered simultaneously during the design procedure. This flexibility will be used below to improve the robustness properties of our proposed design scheme.

Preliminary LTI Robustness Analysis

After an initial controller has been obtained as the solution of the above multi-objective design problem, closer attention is now paid to the validity of a few approximations that were made and their potential impact on the closed-loop behavior. More precisely, it is shown here how LTI robustness analysis tools (such as μ or skew-f bounds) can be used to detect potential difficulties induced by three main sources of uncertainties.

Plant uncertainties

When combining Equations (7) and (1) to obtain (8), it is assumed that both f and G are well known. However, in practice, uncertainties δ are always present so that Equation (8) is now written as:

$$\dot{x} = A(\delta)x + B(\delta)L_A(v) + w \tag{16}$$

where $\delta = \left[\delta_1 \dots \delta_l\right]^T \in \mathbb{R}^l$. Assuming that both A and B rationally depend on δ, it is then possible through an LFT modeling approach [14] to rewrite $\Sigma(s)$ as the following Linear Fractional Representation (LFR), as depicted in Figure 2:

$$\Sigma(s) = \mathcal{F}_u\left(M(s), \Delta_M\right) \tag{17}$$

where $\mathcal{F}_u(.)$ denotes the upper Linear Fractional Transformation (LFT), $M(s)$ is an LTI system and:

$$\Delta_M \in \Delta_M = \left\{ diag\left(\delta_1 I_{k_1}, \dots, \delta_l I_{k_l}\right), \delta_i \in \mathbb{R} \right\} \tag{18}$$

Actuator uncertainties

In Assumption 1, the commutative property (6) might not be valid in all cases. Following [5], it is then proposed to relax it as follows.

Assumption 2

There exist a nonlinear bounded operator $\Gamma(.)$ *and a positive bound* $k_\Gamma \in \mathbb{R}^+$ *such that* $\forall \upsilon(t) \in \mathbb{R}^m$*:*

$$L_A\left(\Lambda^{-1}\upsilon(t)\right) = \Lambda^{-1}L_A\left(\upsilon(t)\right) + \Gamma\left(\upsilon(t)\right) \tag{19}$$

$$\left\| \Gamma\left(\upsilon(t)\right) \right\| \le k_\Gamma \left\| \upsilon(t) \right\| \tag{20}$$

It results from Assumption 2 that the linear model $\Sigma_A(s)$ in Figure 1 should now be replaced by the nonlinear uncertain version $\Sigma_A(s) + \Gamma(.)$, as illustrated in Figure 2.

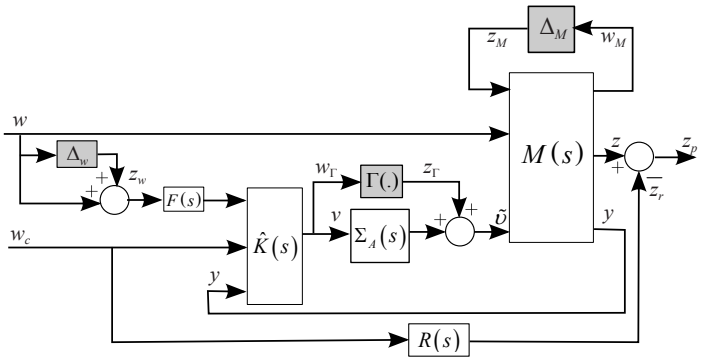

Figure 2 – Closed-loop scheme for LTI stability analysis.

Estimation uncertainties

Finally, one should notice that only an estimated $\hat{w}$ of the nonlinear input perturbations w is available to the outer-loop controller $\hat{K}(s)$. While this estimation process has been taken into account in the design phase through the approximation $\hat{w} \approx F(s)w$, it might be too optimistic in practice. A diagonal perturbation block Δ_w will then be considered to introduce some multiplicative uncertainties on the signal so that $\hat{w}$ is now transformed into $\left(I + \Delta_w\right)\hat{w}$. This is also visualized in the robustness analysis diagram in Figure 2.

As is usual in any standard LFT modeling process, the three uncertain blocks that have been described above are normalized, merged into a single block-diagonal operator $\Delta = diag\left(\Delta_M, \Gamma(.), \Delta_w\right)$ and pulled out to generate an augmented linear model $P(s)$. These operations are summarized in Figure 3. The APRICOT Library from the Matlab

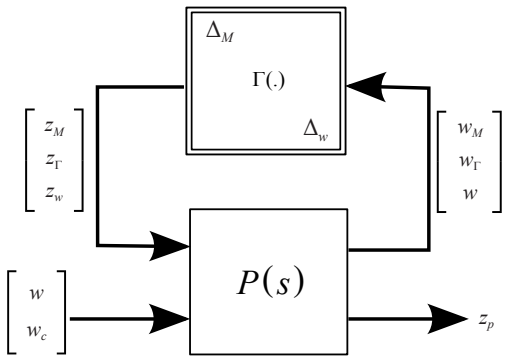

Figure 3 – LFT of the system for LTI robustness analysis.

Toolbox SMAC [22] can be used to generate such an LFT, from a set of LTI models.

Temporarily assuming that Δ is a time-invariant operator, μ or skew-μ analysis can be used to quantify, respectively, the stability and performance properties of the uncertain closed-loop depicted in Figure 3. Using the SMART Library from the Matlab Toolbox SMAC [22] allows bounds on the structured singular value [24] to be computed. Since Δ has been normalized, the system is said to be robustly stable to LTI perturbations if the μ upper-bound verifies $\overline{\mu} < 1$. Otherwise, a destabilizing worst-case perturbation Δ^* might exist such that $\overline{\sigma}(\Delta^*) < 1$.

Multi-model Design

Using the above robustness analysis results, two main ways exist to improve the initial controller $\hat{K}(s)$. Since it was designed within the H_∞ framework, a natural way consists in using a μ-synthesis approach. While this strategy, already implemented in MATLAB™ [26], works well in the case of complex-valued uncertainties, numerical difficulties are often reported with real-valued uncertain parameters. Moreover, results might be quite conservative in that case. For these reasons, the alternative path, consisting of a multi-model design approach, will be preferred next. First considered in [1], this intuitive approach leads to non-convex optimization problems. However, as has been already pointed out, it has regained interest recently thanks to the flexibility of non-smooth H_∞ optimization algorithms. The latter indeed offer new perspectives in this direction, since multiple models can be considered simultaneously. From this observation, a simple iterative algorithm can be proposed. Starting from a single-model design, the principle consists of analysis & multi-model design iterations. During the analysis step, worst-case configurations (associated with Δ^*) are isolated, in order to enrich the bank of models to be considered in the next design step. This is summarized below.

Algorithm 1
Robust multi-model design

1. Define a nominal configuration model $\Sigma_0(s)$ using the input linearizing inner-loop control law (7), leading to (8).

2. Set $i = 0$ and solve (14)-(15) to compute an initial controller $\hat{K}_0(s)$.

3. Perform LFT modeling & robustness analysis pursuant to previous Subsection. Extract a destabilizing perturbation Δ_i^*. If $\overline{\sigma}(\Delta_i^*) < 1$, then go to Step 4, otherwise go to Step 5.

4. Enrich the bank of models with Δ_i^*, set $i \leftarrow i+1$, compute $\hat{K}_i(s)$ via multi-model H_∞ design and return to Step 3.

5. Perform a final robustness analysis with μ upper-bound evaluation.

Remark 2
Unlike μ-synthesis based approaches, the above algorithm implements necessary conditions for robust stability with respect to LTI perturbations, which become sufficient if the μ upper-bound in Step 1) is less than 1.

Towards a Global Robustness Analysis

In the simplified robustness analysis approach of page 3, the nonlinear input signal w is considered as an external perturbation. Yet, considering Equations (8) and (9), it is clear that w may depend on x and θ_p in a quite complicated way. Consequently, robustness analysis becomes tricky in the most general case. Fortunately, with a good knowledge of the studied process, reasonably simpler approximations can be obtained in practice, such as:

$$w = H(\theta_p)x + W(x) \tag{21}$$

with the following assumptions:

- $H(.)$ is assumed to depend rationally on θ_p, and can thus be rewritten as an LFT.
- the nonlinear operator $W(x)$ satisfies Lipschitz conditions.

Hence, the LFT $F_u(P(s),\Delta)$ of Figure 3 – further denoted $F_u(\tilde{P}(s),\tilde{\Delta})$ – is modified to include additional blocks in $\tilde{\Delta}$ so that w will no longer appear as an external perturbation:

$$\tilde{\Delta} = diag\left(\Delta_M, \Gamma(.), \Delta_w, W(.), \Theta_p\right) \tag{22}$$

The extended uncertain operator $\tilde{\Delta}$ now clearly contains uncertainties Δ_M, Δ_w and time-varying parameters Θ_p as well as memoryless nonlinearities $\Gamma(.)$ and $W(.)$. Robustness analysis then must be performed with more general tools based, for example, on the IQC framework [16].

Application to longitudinal aircraft control design

The above robust nonlinear compensation framework is now applied to a longitudinal aircraft control problem. Note that the lateral motion is not yet considered, assuming a steady flat-wing aircraft with no sideslip. Lateral controller design will be described while global simulations with both combined motions will be presented.

Nonlinear Longitudinal Aircraft Model

The longitudinal motion of a civil aircraft can be described by the following 4-state model [7]:

$$\begin{cases} m\dot{V} &= -\overline{q}S\hat{C}_D(\alpha) - mg\sin\gamma + F\cos\alpha \\ mV\dot{\gamma} &= \overline{q}S\hat{C}_L(\alpha,q,V,\delta_e) - mg\cos\gamma + F\sin\alpha \\ J\dot{q} &= \overline{q}SL\hat{C}_m(\alpha,q,V,\delta_e) + z_e F \\ \dot{\theta} &= q \end{cases} \tag{23}$$

where V is the airspeed, γ is the flight path angle, q is the pitch rate, θ is the pitch angle, $\bar{q} = \frac{1}{2}\rho V^2$ is the dynamic pressure, J is the longitudinal inertia, m is the mass, S is the reference surface, L is the reference length (often taken as the half span), ρ is the air density, α is the angle of attack ($\alpha = \theta - \gamma$), F is the engine thrust on the longitudinal axis and z_e is the vertical shift between the position of the center of gravity and the thrust application point. The drag, lift and pitching coefficients $\hat{C}_D$, $\hat{C}_L$ and $\hat{C}_m$ can be expressed as follows:

$$\begin{aligned} \hat{C}_D(\alpha) &= C_{D0} + C_{D\alpha}\alpha + C_{D\alpha 2}\alpha^2 \\ \hat{C}_L(\alpha,q,V,\delta_e) &= \underbrace{C_{L0} + C_{L\alpha}\alpha + C_{Lq}\frac{q}{V}}_{\tilde{C}_L} + C_{L\delta_e}\delta_e \\ \hat{C}_m(\alpha,q,V,\delta_e) &= \underbrace{C_{m0} + C_{m\alpha}\alpha + C_{mq}L\frac{q}{V}}_{\tilde{C}_m} + C_{m\delta_e}\delta_e \end{aligned} \quad (24)$$

where δ_e is the elevator deflection angle and the C_{xy} are fixed aerodynamic coefficients, whose values can be obtained from the benchmark library of the SMAC Toolbox[1] and do not depend on the Mach number. Here $\xi = [V\ \gamma\ q\ \theta]^T$, $u = [F\ \delta_e]^T$ and $\theta_p = [m\ x_{cg}\ V_0]^T$, where x_{cg} is the center of gravity position and V_0 is the initial airspeed. The operating domain for a landing application is such that $V \in [60\ 90] m/s$, $m \in [123\ 180] tons$ and $x_{cg} \in [15\ 41]\%$, defining the admissible set Θ. F and δ_e follow the first-order actuator dynamics $\Sigma_A(s)$:

$$\Sigma_A(s) = \begin{pmatrix} \frac{1}{2s+1} & 0 \\ 0 & \frac{1}{0.07s+1} \end{pmatrix} \quad (25)$$

Remark 3

Using first-order models for the actuators is common practice in the aeronautical industry, and it is sufficiently representative here. However, rate limitations are neglected, but it would be possible to add an anti-windup controller to take them into account.

The aerodynamic coefficients can have up to 30% of multiplicative uncertainties. Using the notation of (1) and applying (5) from Assumption 1, (23) is rewritten the same way with:

$$f = \begin{pmatrix} \frac{-\bar{q}SC_D}{m} - g\sin\gamma \\ \frac{\bar{q}S\tilde{C}_L}{mV} - \frac{g}{V}\cos\gamma \\ \frac{\bar{q}SL}{J}\tilde{C}_m \\ q \end{pmatrix} \qquad B = \begin{pmatrix} 1 & 0 & 0 & 0 \\ 0 & 0 & 1 & 0 \end{pmatrix}^T$$

$$\Lambda = \begin{pmatrix} \frac{\cos\alpha}{m} & 0 \\ \frac{z_e}{J} & \frac{\bar{q}SL}{J}C_{m_{\delta_e}} \end{pmatrix} \qquad \Delta_G = \begin{pmatrix} 0 & 0 \\ \frac{\sin\alpha}{mV} & \frac{\bar{q}S}{mV}C_{L_{\delta_e}} \\ 0 & 0 \\ 0 & 0 \end{pmatrix}$$

Remark 4

Given the operating domain of the system, Λ is non-singular. Furthermore, Λ is slowly varying, since its dynamics mainly come from the dynamic pressure $\bar{q}$. These two conditions verify Assumption 1.

[1] http://w3.onera.fr/smac/

Remark 5

The choice of B was made based on the maximum control efficiency. Indeed, as is clear from (23), the thrust input F mainly affects the airspeed V, and the elevator deflection δ_e has a large impact on the pitch rate q.

The goal is to track the airspeed V and the flight path angle γ, and the state is assumed to be fully available to the controller, yielding $C = I$. The reference model $R(s)$ for the airspeed (1st order dynamics) and the flight path angle (3rd order dynamics) is given by:

$$R(s) = \begin{pmatrix} \frac{1}{6.5s+1} & 0 \\ 0 & \frac{0.35^2}{(2s+1)(s^2+2*0.7*0.35s+0.35^2)} \end{pmatrix} \quad (26)$$

Nonlinear Compensation Technique

Using the previous notation it is now possible to apply the method described in page 2. First applying the control input (7) leads to the linearized system (8). $\hat{\zeta}$ is chosen so that w_f only preserves the nonlinear terms on the flight path angle dynamics γ, canceling the nonlinear dynamics on V_a and q. The nominal configuration $\bar{\theta}_p$ is set for a mass of 150 tons, a center of gravity position at 21%, an initial airspeed of 70 m/s and an altitude of 300 m (landing configuration). This configuration is "central" in terms of the system pole location, ensuring that the other configurations are covered as much as possible when designing the robust controller. Choosing a worst-case configuration could also be a possibility, but the nominal performance is highly degraded in this case and the "opposite" worst-case configurations may be harder to control. According to the specifications of the robust nonlinear compensation technique; the frequency weightings $W_p(s)$ and $W_u(s)$ are chosen respectively as low-pass and high-pass filters:

$$W_p(s) = \begin{pmatrix} \frac{s/2+0.15}{s+1.5\times10^{-4}} & 0 \\ 0 & \frac{s/20+0.40}{s+4\times10^{-4}} \end{pmatrix} \quad (27)$$

$$W_u(s) = \begin{pmatrix} \frac{s+2}{0.001s+20} & 0 \\ 0 & \frac{s+0.2}{0.001s+2} \end{pmatrix} \quad (28)$$

The filter $F(s)$ is such that:

$$F(s) = \begin{pmatrix} \frac{0.1}{2s+1} & 0 & 0 & 0 \\ 0 & \frac{1}{2s+1} & 0 & 0 \\ 0 & 0 & \frac{0.1}{2s+1} & 0 \\ 0 & 0 & 0 & 0 \end{pmatrix} \quad (29)$$

The second term in (29) on the diagonal is higher than the others, since it is not compensated by the input signal $\hat{\zeta}$ (which only compensates for the first and the third nonlinear terms). This enables the controller to focus more on this one than on the others. The last term is 0 since the last equation in (23) does not contain any nonlinear terms.

A third-order controller is chosen, since it offers a good compromise between the achievable performance and a preferable low-order controller for easier implementation. Solving the multi-objective H_∞ minimization problem (14)-(15) with the routine hinfstruct of the Robust Control Toolbox for Matlab [3] yields an H_∞-norm of $\gamma_\infty = 0.9653$ after a few iterations, thus insuring that the frequency-domain

specifications are fulfilled. Nonlinear simulations are performed with the obtained initial controller $\hat{K}_0(s)$, and the corresponding results are depicted in Figure 4 and Figure 5.

In Figure 4, the aircraft responses to a 3 degree step demand on the flight path angle γ are visualized for various configurations of mass $\in \{120,150,180\}$ tons, initial airspeed $V \in \{60,70,80\}$ m/s, and center-of-gravity locations $x_{cg} \in \{15,20,40\}$%.

Similarly, the responses to a 3 m/s variation step demand on the longitudinal airspeed V are shown in Figure 5. In both cases, the dashed red plots correspond to the reference signals to be tracked.

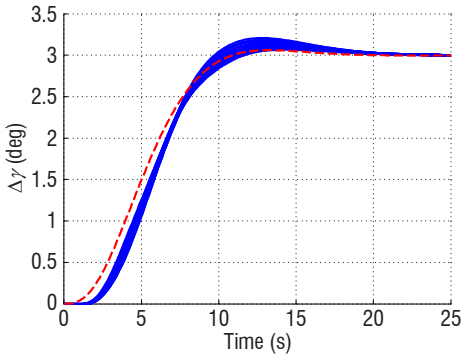

(a) Flight path angle vs. time

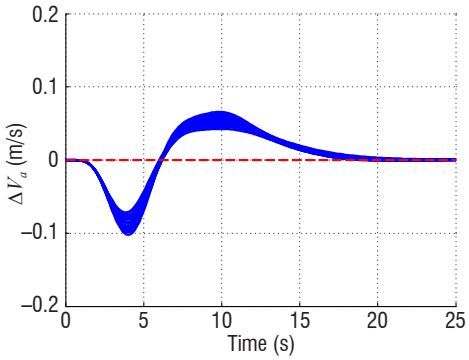

(b) Airspeed vs. time

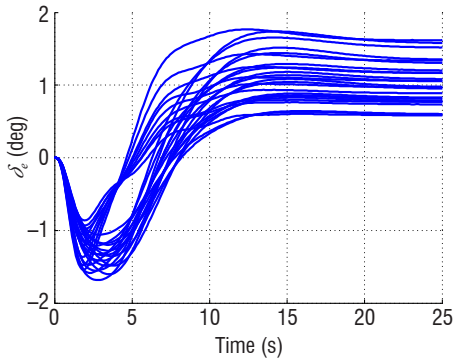

(c) Elevator deflection vs. time

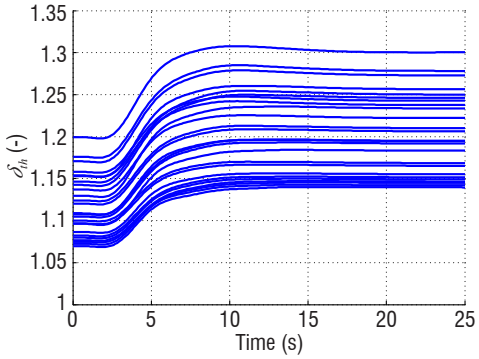

(d) Thrust factor vs. time

Figure 4 – Nonlinear Simulations with a 3° step on γ, for different initial aircraft configurations and no aerodynamic coefficient uncertainties, with the initial controller $\hat{K}_0(s)$.

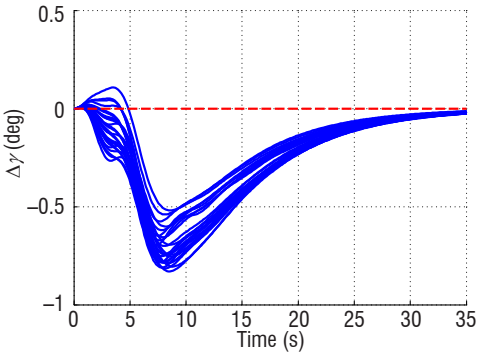

(a) Flight path angle vs. time

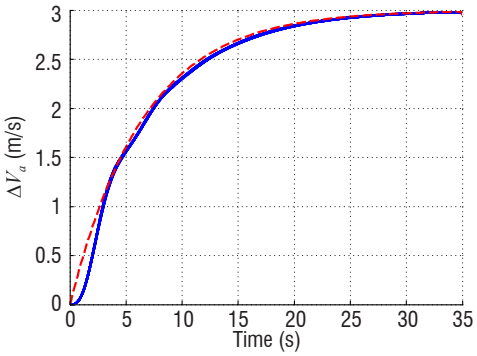

(b) Airspeed vs. time

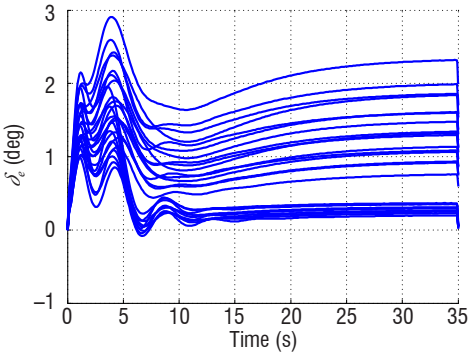

(c) Elevator deflection vs. time

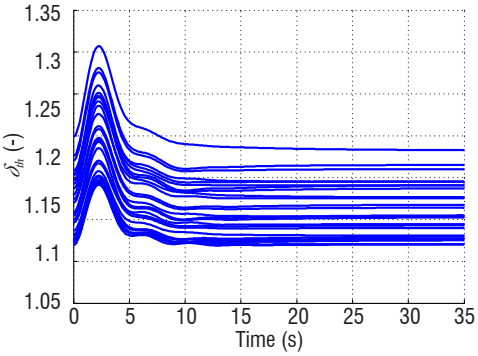

(d) Thrust factor vs. time

Figure 5 – Nonlinear Simulations with a 3 m/s step on V, for different initial aircraft configurations and no aerodynamic coefficient uncertainties, with the initial controller $\hat{K}_0(s)$.

Both simulations prove the effectiveness of the robust nonlinear compensation scheme with regard to performance and robustness properties. The flight domain is indeed very large thanks to the nonlinear compensation part of the controller being aimed at maintaining as much as possible the nominal performance. The controller manages to follow the reference models quite well, while also ensuring a good decoupling. Note however that no uncertainties in the aerodynamic coefficients have been considered yet. These will have significant impact on the performance and stability of the system, as will be shown in the next section dealing with robust stability analysis.

Robustness analysis and multi-model design

The above controller $\hat{K}_0(s)$ has been designed to cope with a large operating domain under nominal conditions. The uncertain operators represented by "gray boxes" in Figure 2 have thus not been considered yet. The objective of this section is twofold. First, the effects of the aforementioned uncertainties are studied within the LTI frameworks with the help of μ-analysis tools. Next, the identified worst cases are used in a multi-model design strategy detailed in Algorithm 1 to improve the robustness properties of the initial controller.

LTI modeling and μ-analysis

LFT modeling is a key step in our robustness analysis process. Starting from the set of nonlinear equations (23), parametric uncertainties are first introduced in the aerodynamic coefficients:

$$C_D = \left(1+\delta_{C_D}\right)\hat{C}_D$$

$$C_L = \left(1+\delta_{C_L}\right)\hat{C}_L$$

$$C_m = \left(1+\delta_{C_m}\right)\hat{C}_m$$

and variations are also introduced in the airspeed V, mass m and center of gravity location: $V = V_0 + \delta_V$, $m = m_0 + \delta_m$, $x_{cg} = x_{cg_0} + \delta_{x_{cg}}$. Next, the equations are linearized so that a bank of parameter-dependent linear models, as described in (16), is obtained. From this continuous set, a low-order LFT model $\mathcal{F}_u\left(M(s),\Delta_M\right)$ (see Eq. (17)) is rather easily obtained with the help of the most recent algorithms implemented in the APRICOT Library of the SMAC Toolbox [23]. These algorithms, using orthogonal least square techniques, are based on low-order polynomial interpolation methods. For this application the size of the Δ_M-block is kept reasonably low:

$$\Delta_M = \mathrm{diag}\left(\delta_V I_6, \delta_{C_D} I_2, \delta_{C_L} I_3, \delta_{C_m} I_2, \delta_m I_1, \delta_{x_{cg}} I_1\right) \in \mathbb{R}^{15\times 15}$$

As a result, the size of the global Δ-block including $\Gamma(.)$ and Δ_w (see Figure 3) verifies:

$$\Delta = \mathrm{diag}\left(\Delta_M, \Delta_w, \Delta_\Gamma\right) \in \mathbb{R}^{20\times 20}$$

A normalization step is finally applied so that variations of Δ in the unit ball induce 30% uncertainties in the aerodynamic coefficients, and 30% variations in Δ_w and Δ_Γ. Note that this last step is easily achieved with the LFT modeling library available in the SMAC Toolbox. Based on this normalized LFT object, both upper and lower bounds of the structured singular value μ are evaluated with the SMART Library of the SMAC Toolbox. With the nominal controller $\hat{K}_0(s)$, a lower-bound $\underline{\mu}_\Delta > 1$ is found together with its corresponding worst-case configuration Δ_1^* such that $\bar{\sigma}\left(\Delta_1^*\right) = \underline{\mu}_\Delta^{-1} < 1$.

Multi-model design

Following step 4 of Algorithm 1, Δ_1^* is used to initialize our multi-model design procedure. Note that this case corresponds to a retracted position of the center of gravity, maximum weight and high values of the aerodynamic coefficient uncertainties. After 5 more iterations, a new controller $\hat{K}(s)$ is obtained that significantly improves the worst-case configuration. For this controller one indeed obtains $\underline{\mu}_\Delta < 1$. However, using standard algorithms, the upper-bound $\bar{\mu}_\Delta$ remains above 1, which does not make it possible to conclude on stability. Refined versions of the algorithm using branch-and-bound techniques [17], now available in the SMART Library, are then used, which greatly improves the accuracy of the upper-bound. One eventually obtains $\bar{\mu}_\Delta < 1$, as is summarized in Table 1.

Controller	Lower-bound $\underline{\mu}_\Delta$	Upper-bound $\bar{\mu}_\Delta$
Nominal – DG-scaling	1.4610	1.5110
Multi-model – DG-scaling	0.8957	1.0780
Multi-model – branch-and-bound	0.8999	0.9449

Table 1 – Values of the μ-bounds for the nominal and multi-model controllers. The computations for the multi-model controller are made using the initial DG-scaling method and the improved branch-and-bound algorithm.

Time-domain evaluation

To conclude this section, a few nonlinear simulations are performed with the above multi-model based controller. The flight path angle (γ) and airspeed (V) step demands are first applied for various aircraft configurations without uncertainties. The results, to be compared with those obtained with the nominal controller, are displayed in Figures 6 and 7.

As expected, the decoupling is a bit degraded and the responses are slightly slower but major improvements will be shown in the presence of uncertainties.

Let us now introduce 25% uncertainties in the aerodynamic coefficients (not 30%, so that the nominal controller is not completely unstable). The aircraft responses to a step demand on γ are visualized in Figure 8. The left subplot (Figure 8a) reveals poor robustness properties of the nominal controller, while significant improvements are clearly observed on the right subplot (Figure 8b) with the multi-model controller. This clearly demonstrates the efficiency of the proposed methodology.

Application to lateral aircraft control design

Now that the method has been successfully applied on the longitudinal part of the aircraft, the lateral part will be dealt with using the exact same strategy as explained below.

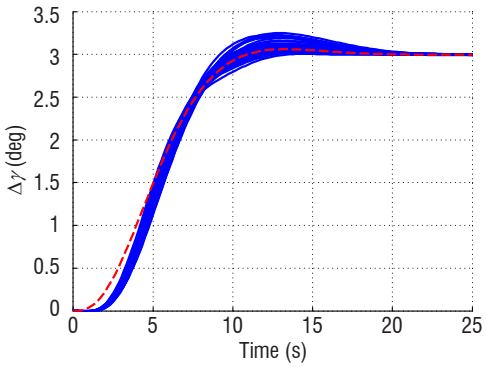

(a) Flight path angle vs. time

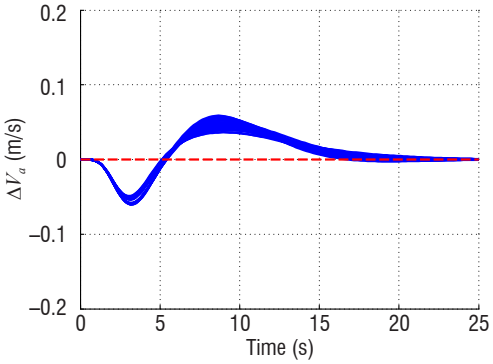

(b) Airspeed vs. time

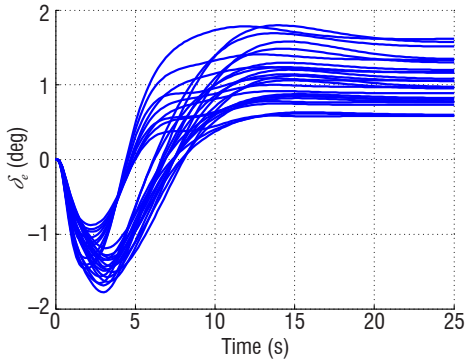

(c) Elevator deflection vs. time

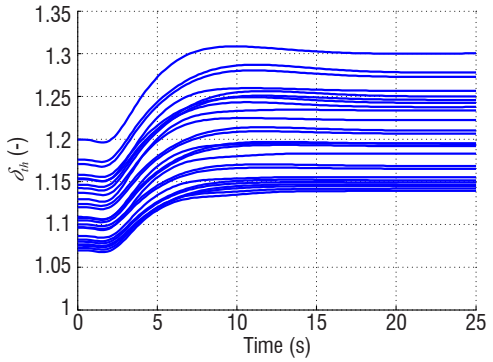

(d) Thrust factor vs. time

Figure 6 – Nonlinear Simulations with a 3° step on γ, for different initial aircraft configurations and no aerodynamic coefficient uncertainties, with the multi-model controller $\hat{K}(s)$.

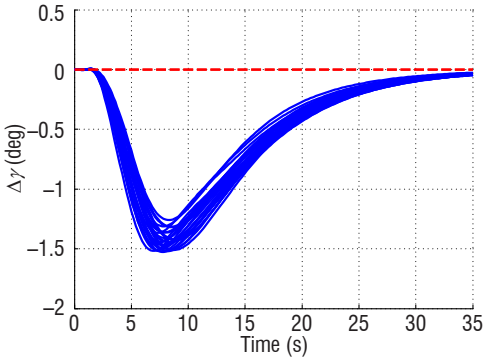

(a) Flight path angle vs. time

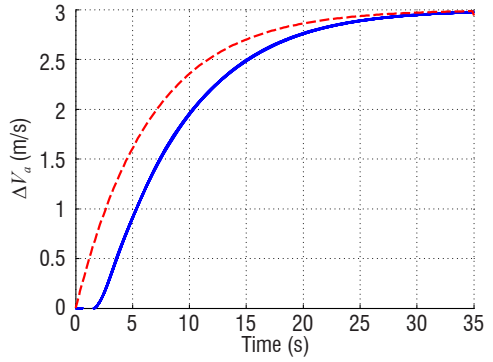

(b) Airspeed vs. time

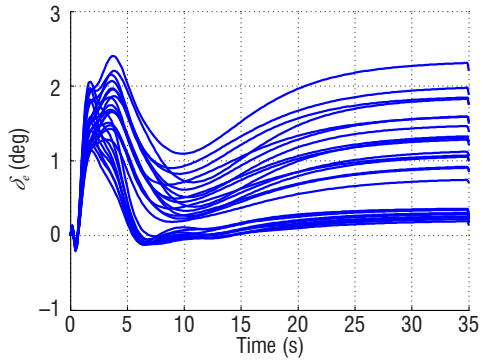

(c) Elevator deflection vs. time

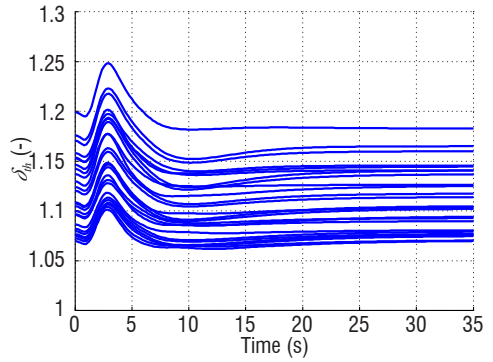

(d) Thrust factor vs. time

Figure 7 – Nonlinear Simulations with a 3 m/s step on V, for different initial aircraft configurations and no aerodynamic coefficient uncertainties, with the multi-model controller $\hat{K}(s)$.

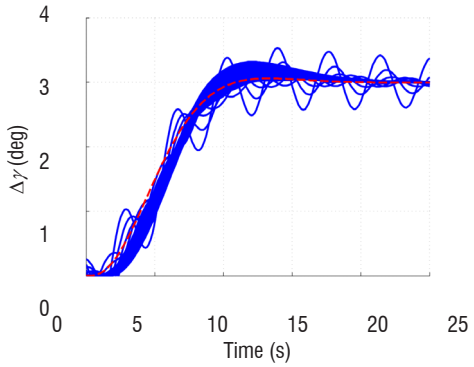

(a) γ step responses for the nominal controller

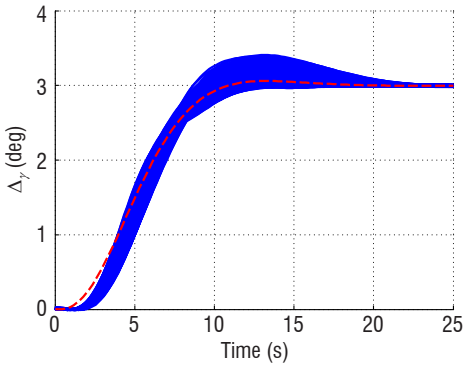

(b) γ step responses for the multi-model controller.

Figure 8 – Comparison between the nominal controller $\hat{K}_0(s)$ (a) and the multi-model controller $\hat{K}(s)$ (b) for all admissible configurations with ±25% of uncertainties: γ step responses versus time.

Nonlinear Lateral Aircraft Model

The lateral motion of a civil aircraft can be described by the following 4-state model [7]:

$$\begin{cases} mV\dot{\beta} &= mV\left(p\sin\alpha - r\cos\alpha\right) + mg\left(\sin\theta\cos\alpha\sin\beta \right. \\ &\quad + \cos\theta\sin\phi\cos\beta - \cos\theta\sin\alpha\cos\phi\sin\beta \\ &\quad \left. + \bar{q}S\hat{C}_Y - F\sin\beta\cos\alpha \right. \\ \dot{\phi} &= p + \tan\theta\left(q\sin\phi + r\cos\phi\right) \\ I_{zz}\dot{r} &= \bar{q}SL\hat{C}_n + \left(I_{xx} - I_{yy}\right)pq \\ I_{xx}\dot{p} &= \bar{q}SL\hat{C}_l + \left(I_{yy} - I_{zz}\right)rq \end{cases} \tag{30}$$

where β and ϕ are, respectively, the sideslip and roll angles, p and r are the roll and yaw rates, and I_{xx} and I_{zz} are the inertias along the x-body and z-body axes. The side force, roll and yaw coefficients $\hat{C}_Y$, $\hat{C}_l$ and $\hat{C}_n$ are expressed as follows:

$$\begin{aligned} \hat{C}_Y &= \underbrace{C_{Y_\beta}\beta}_{\tilde{C}_Y} + C_{Y_r}\delta_r \\ \hat{C}_l &= \underbrace{C_{l_\beta}\beta + \frac{L}{V}\left(C_{l_p}p + \left(C_{l_{r_0}} + C_{l_{r_\alpha}}\alpha\right)r\right)}_{\tilde{C}_l} + C_{l_{\delta_a}}\delta_a + C_{l_{\delta_r}}\delta_r \\ \hat{C}_n &= \underbrace{(C_{n_{\beta_0}} + C_{n_{\delta_\alpha}})\beta + \frac{L}{V}\left(C_{n_r}r + (C_{n_{p0}} + C_{n_{p\alpha}}\alpha)p\right)}_{\tilde{C}_n} \\ &\quad + C_{n_{\delta_a}}\delta_a + C_{n_{\delta_r}}\delta_r \end{aligned} \tag{31}$$

where δ_a and δ_r are the aileron and rudder deflection angles, and the C_{xy} are aerodynamic coefficients specific to the given aircraft. Using similar notations to those used in the longitudinal case, let us define: $\xi = [\beta\ \phi\ r\ p]^T$, $u = [\delta_a\ \delta_r]^T$ and $\theta_p = [m\ x_{cg}\ V_0]^T$. δ_a and δ_r follow the first-order actuator dynamics $\Sigma_A(s)$:

$$\Sigma_A(s) = \begin{pmatrix} \frac{1}{0.06s+1} & 0 \\ 0 & \frac{1}{0.2s+1} \end{pmatrix} \tag{32}$$

Using the notation of (1) and applying (5) from Assumption 1, (23) is rewritten in the same way with:

$$\Lambda = \begin{pmatrix} \frac{\bar{q}SL}{I_{zz}}C_{n_{\delta_a}} & \frac{\bar{q}SL}{I_{zz}}C_{n_{\delta_r}} \\ \frac{\bar{q}SL}{I_{xx}}C_{l_{\delta_a}} & \frac{\bar{q}SL}{I_{xx}}C_{l_{\delta_r}} \end{pmatrix}$$

$$\Delta_G = \begin{pmatrix} 0 & \frac{\bar{q}S}{mV}C_{Y_r} \\ 0 & 0 \\ 0 & 0 \\ 0 & 0 \end{pmatrix}$$

$$f = \begin{pmatrix} p\sin\alpha - r\cos\alpha + \frac{g}{V}(\sin\theta\cos\alpha\sin\beta + \cos\theta\sin\phi\cos\beta - \cos\theta\sin\alpha\cos\phi\sin\beta) + \frac{\bar{q}S}{mV}\tilde{C}_Y - \frac{F}{V}\sin\beta\cos\alpha \\ p + \tan\theta\left(q\sin\phi + r\cos\phi\right) \\ \frac{\bar{q}SL}{I_{zz}}\tilde{C}_n + \frac{I_{xx} - I_{yy}}{I_{zz}}pq \\ \frac{\bar{q}SL}{I_{xx}}\tilde{C}_l + \frac{I_{yy} - I_{zz}}{I_{xx}}rq \end{pmatrix}$$

$$B = \begin{pmatrix} 0 & 0 & 1 & 0 \\ 0 & 0 & 0 & 1 \end{pmatrix}^T$$

The goal is to track the roll and sideslip angles ϕ and β, respectively. The reference model $R(s)$ is given by:

$$R(s)=\begin{pmatrix} \frac{1}{\frac{s^2}{0.80^2}+\frac{2*0.75}{0.80}s+1} & 0 \\ 0 & \frac{1}{\frac{s^2}{0.75^2}+\frac{2*0.75}{0.75}s+1} \end{pmatrix} \quad (33)$$

Remark 6

Note that some longitudinal state variables are present in the lateral dynamics equations. For the computation of the lateral controller it will be assumed that these variables maintain a predefined equilibrium. The simulations will be performed on the full model with the previous satisfactory longitudinal controller, in order to maintain the longitudinal equilibrium despite the lateral motion.

Lateral Controller Design

The same method as for the computation of the longitudinal controller is used here (some details will be omitted). The nominal configuration $\overline{\theta}_p$ is the same as before. For the lateral case, the frequency weightings used for the H_∞-design procedure $W_p(s)$ and $W_u(s)$ are chosen respectively as:

$$W_p(s)=\begin{pmatrix} \frac{s/5+2.5}{s+2.5\times10^{-3}} & 0 \\ 0 & \frac{s/5+1}{s+1\times10^{-3}} \end{pmatrix} \quad (34)$$

$$W_u(s)=\begin{pmatrix} \frac{s+2}{0.001s+20} & 0 \\ 0 & \frac{s+0.5}{0.001s+5} \end{pmatrix} \quad (35)$$

The filter $F(s)$ is such that: (see the explanations for the choice of (29) for a better understanding)

$$F(s)=\begin{pmatrix} \frac{1}{s+1} & 0 & 0 & 0 \\ 0 & \frac{1}{s+1} & 0 & 0 \\ 0 & 0 & \frac{0.02}{s+1} & 0 \\ 0 & 0 & 0 & \frac{0.02}{s+1} \end{pmatrix} \quad (36)$$

For the same reasons as for the longitudinal controller, a second-order controller is chosen. Solving the multi-objective H_∞ minimization problem (14)-(15) with the routine hinfstruct of the Robust Control Toolbox for Matlab [3] yields a H_∞-norm $\gamma_\infty = 1.03$ after a few iterations. The stability of the closed-loop system with the initial "nominal" controller $\hat{K}_0(s)$ is checked. Using the same strategy as for the longitudinal case, an LFT is computed yielding a "Δ-block" of dimension 24 x 24. Then, both the upper and the lower bounds of the structured singular value μ are evaluated yielding $\mu_\Delta \in [1.007\ 1.118]$ which does not prove stability. Following Algorithm 1, after 3 iterations, the final controller $\hat{K}(s)$ greatly improves the worst-case stability since now $\mu_\Delta \in [0.7948\ 0.8845]$ which proves stability with respect to LTI uncertainties. Note that, unlike the longitudinal case, no branch-and-bound techniques were needed here to reduce the gap between the lower and upper bounds.

Simulations were run for various initial configurations (different values of θ_p) and with $\pm 30\%$ uncertainties on the lateral aerodynamic coefficients (729 runs were executed). As expected, the lateral multi-model controller performs very well as shown in Figures 9

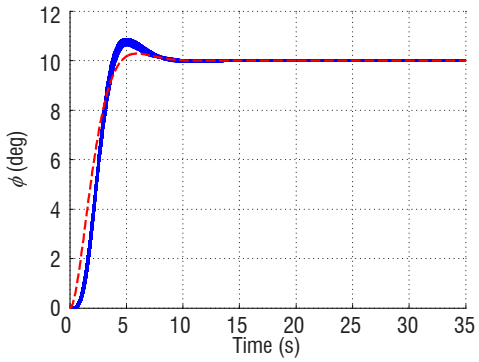

(a) Roll angle vs. time

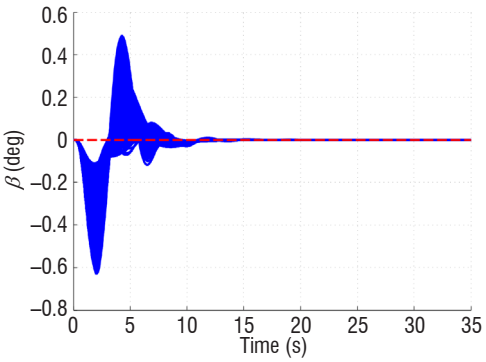

(b) Sideslip angle vs. time

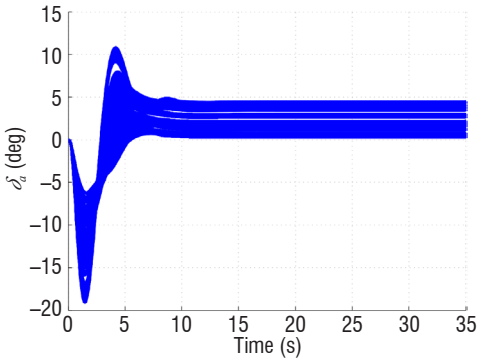

(c) Ailerons deflection vs. time

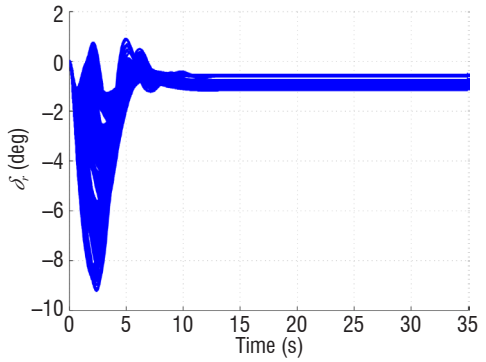

(d) Rudder deflection vs. time

Figure 9 – Nonlinear Simulations with a 10 deg step on ϕ, for various initial aircraft configurations and $\pm 30\%$ aerodynamic coefficient uncertainties, with the lateral multi-model controller 10.

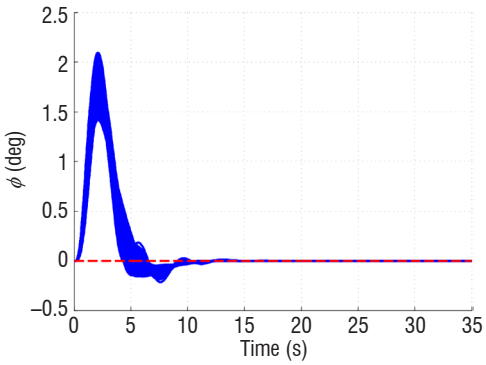

(a) Roll angle vs. time

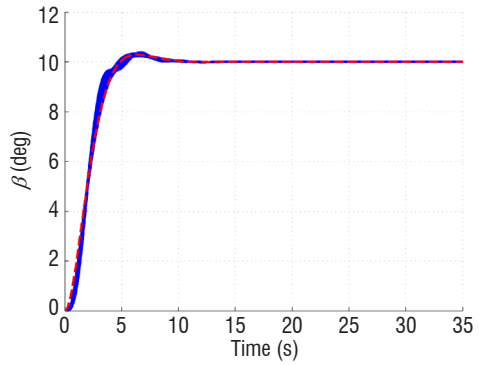

(b) Sideslip angle vs. time

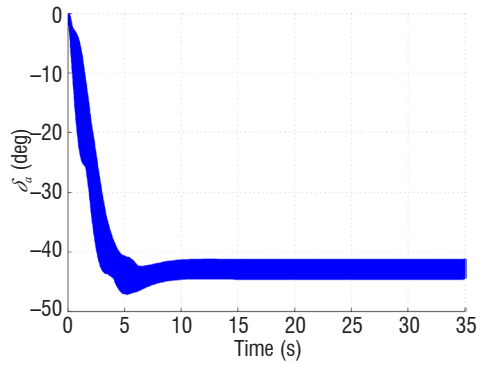

(c) Ailerons deflection vs. time

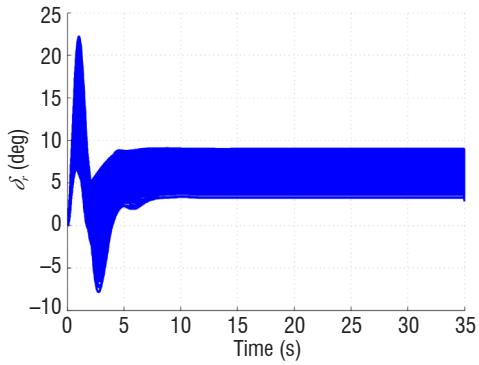

(d) Rudder deflection vs. time

Figure 10 – Nonlinear Simulations with a 10 deg step on β, for various initial aircraft configurations and ±30% aerodynamic coefficient uncertainties, with the lateral multi-model controller $\hat{K}(s)$.

and 10, where respectively the references of the roll and sideslip angles ϕ and β (red dashed line) are well tracked with reasonable control inputs δ_a and δ_r. Furthermore, no sign of even slight instability is present and the decoupling is greatly ensured.

Global application: aircraft landing

Finally, the longitudinal and lateral controllers are tested on a realistic landing application. The Instrument Landing System (ILS) allows the aircraft to operate and automatically land despite difficult weather conditions (e.g., restricted visibility). It is composed of ground-based signal transmitters and on-board receiving equipment. The ground-based equipment, located at the edges of the runway, comprises localizer and glide path radio transmitters and some marker beacons. On board, the receivers allow the emitted radio signals to be processed.

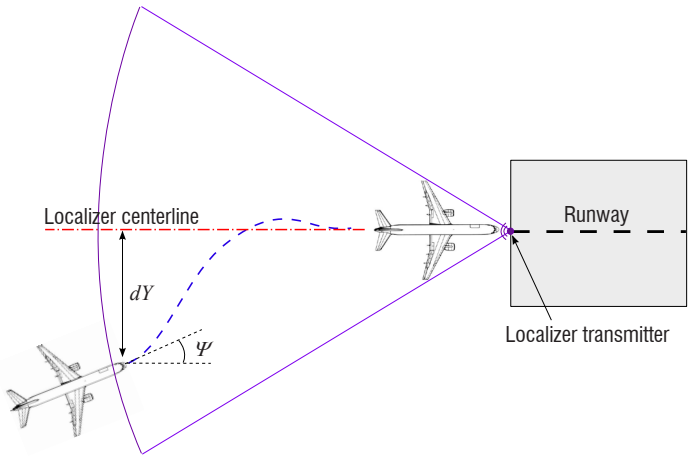

Figure 11 – The localizer beam system for aircraft lateral deviation adjustment.

The glide and localizer signals are the ones of interest for performing an automatic landing. They both allow the position of the aircraft relative to the ideal trajectory for landing to be known. Thus, a guidance control law can be designed so that the aircraft trajectory follows the centerline of the runway with a nominal descent path angle of $\gamma_{nom} = -3$ degrees. The lateral deviation is given by the localizer beam, while the longitudinal deviation is given by the glide beam. Figures 11 and 12 present the principles. Further details on autoland can be found in [13].

The aim is thus to track the glide and localizer signals and to perform the landing, via the addition of simple guidance outer loops which provide necessary inputs orders to the controller. The aircraft must hit the ground with a vertical speed $V_z = [2-3]$ ft/s not further than 500 meters after the runway threshold. Furthermore, if a lateral wind is blowing the aircraft must be able to have a final azimuth angle Ψ of 0° without being out of the axis of the runway during the process.

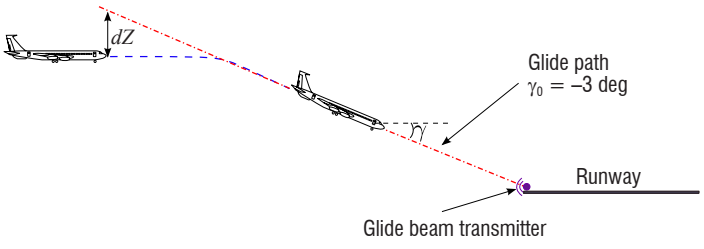

Figure 12 – The glide beam system for aircraft longitudinal deviation adjustment.

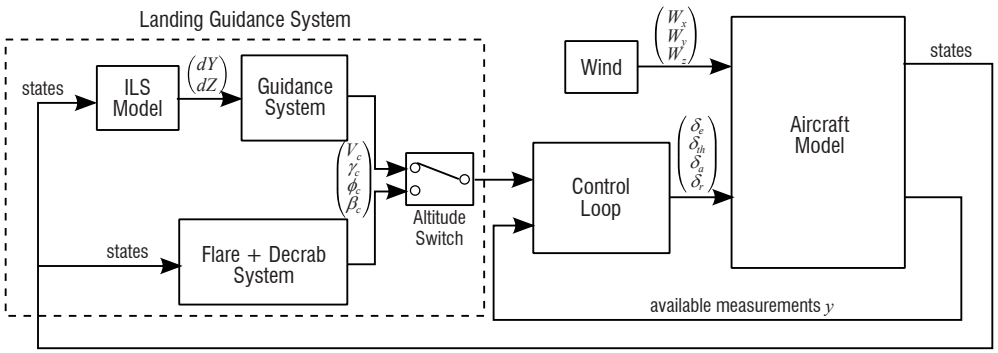

Figure 13 – Guidance and control for landing scheme.

These challenging goals will be verified by running many simulations on the full nonlinear model with, as before, model uncertainties, different initial conditions and wind.

Guidance system

Thanks to an ILS model block the vertical and lateral shifts dZ and dY respectively between the actual position of the aircraft and the glide and localizer signals are recovered. PID controllers, which have as inputs dZ and dY, have been designed to provide the longitudinal and lateral controllers with the necessary values of γ_c and ϕ_c to cancel these shifts. The design is not detailed in the paper, since it really consists of classical design techniques (linearization of the plant from dZ and dY to the controller inputs γ_c and ϕ_c, and PID design from frequency domain specifications). The nominal airspeed will be kept constant ($V = 70$ m/s). The general principle of the landing guidance + control system is given in Figure 13. Note that the flare + decrab control system block will be described in the following subsection.

Flare and decrab phases

Just before landing, thanks to the ILS guidance detailed above, the aircraft should fly with a fixed airspeed of –3° m/s, a flight path angle of –3° and be aligned with the runway. The objective of the flare control system, usually activated at 50 ft (15 m) above ground consists in generating an appropriate slope angle γ_c to be tracked so that the vertical speed at touchdown approaches 2.5 ft/s (0.75 m/s) and the aircraft hits the ground 400 m after the runway threshold. In order to do so, a corresponding trajectory $h(x)$ is determined using some geometric considerations and γ_c is given in real time using the following relation:

$$\dot{h}\left(x(t)\right) = \frac{dh(x)}{dx} V_{gr}(t) = -V(t)\sin\left(\gamma_c(t)\right)$$

(where V_{gr} is the ground speed). The procedure is shown in Figure 14.

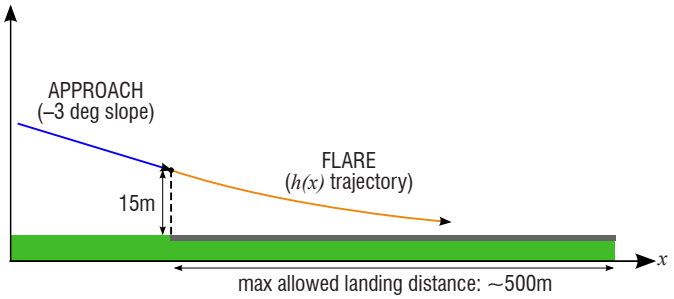

Figure 14 – Trajectory scheme for the flare procedure.

The decrab or align phase, usually activated at 30 ft above the runway, is aimed at setting the azimuth angle Ψ to zero (relative to the azimuth angle of the runway) so that the fuselage is aligned with the runway axis at touchdown. This phase is essential in case of cross wind. It is realized by a PID controller that delivers the appropriate sideslip angle β_c to be tracked as a function of Ψ.

Results

Complete landing simulations, including the flare and decrab phases, are successfully run for different initial conditions with regard to mass, center of gravity position, uncertainties and initial flight path angles. These are shown in Figure 15. Two lateral wind gusts are generated at 35 sec and 55 sec. Arriving above the runway, the azimuth angle is brought back to 0° using the rudder inputs (see Figure 15d). One can check that during this procedure the aircraft does not shift out of the runway when landing (see Figure 15a), and that the wings stay in an horizontal position (Figure 15c). Finally, after having properly recovered the glide reference slope, the flare procedure allows the aircraft to land at around 400 m after the threshold (Figure 15b), while bringing the flight path angle to the proper value allowing the vertical air speed (Figure 15e) to be kept within.

Table 2 summarizes the landing minimum, maximum and mean values for the final azimuth angles ψ, vertical speeds V_z, pitch angles θ, pitch rates X_l and landing distances X_l obtained for every simulation, in order to check whether the landing requirements are met. The main difficult variable to control was the pitch rate q which is not positive but still near 0 deg/s. The other values are within an acceptable range with regard to the mean value and also the standard deviation is not higher than the limits, which shows that the whole method (controller synthesis, guidance laws and flare+decrab laws) is clearly robust to uncertainties and allows a proper landing to be performed under many flight conditions. There are a few extreme condition cases (especially for a maximum amount of uncertainties) for which the objectives are slightly exceeded, but this is not critical (the aircraft still lands safely).

Parameters	min	max	mean	standard deviation	objectives
Azimuth angle Ψ (deg)	–1.06	0.59	0.01	0.32	0±1
Vertical speed V_z (ft/s)	0.88	4.46	2.33	0.82	2.5±1
Pitch angle θ (deg)	–2.81	13.01	3.95	4.19	>0
Pitch rate q (deg/s)	–0.73	0.25	–0.25	0.26	>0
Landing distance X_l (m)	190	567	393	115	$0 < X_l < 500$

Table 2 – Final minimum/maximum/mean values for the relevant landing parameters considering all of the simulations.

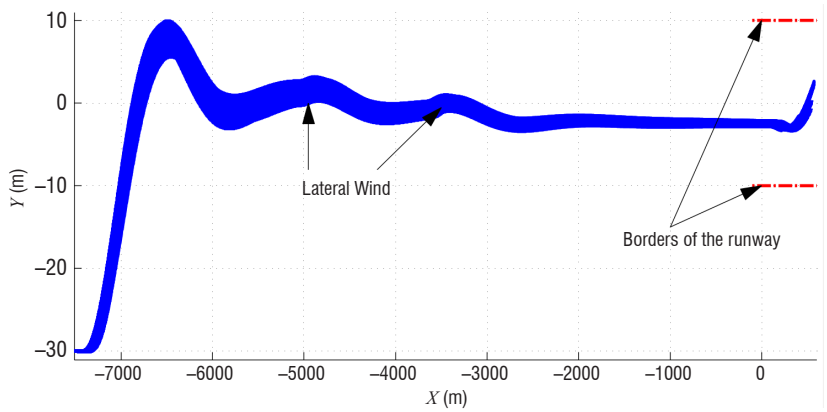

(a) Lateral trajectory

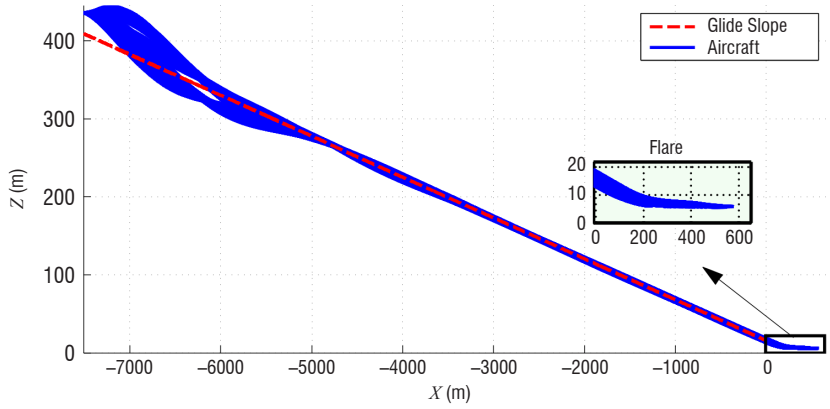

(b) Longitudinal trajectory

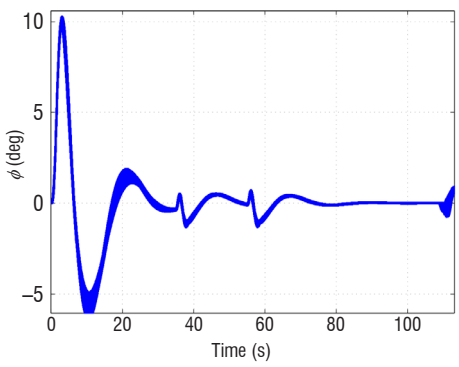

(c) ϕ vs. time

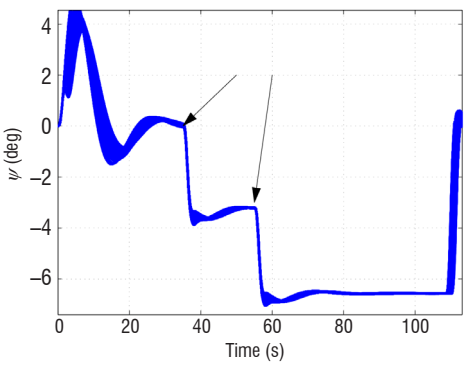

(d) ψ vs. time

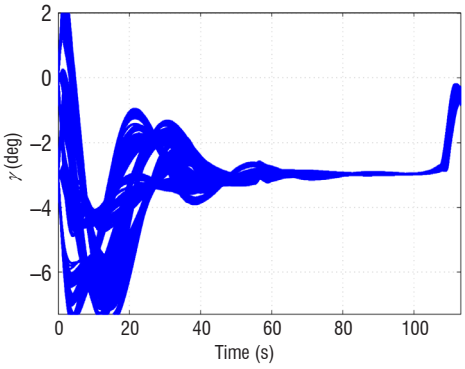

(e) γ vs. time

Figure 15 – Complete landing simulations in the presence of lateral wind, for various initial aircraft configurations.

Conclusion

Inspired by dynamic inversion techniques, an original methodology is proposed in this paper to design nonlinear controllers over possibly large flight envelopes. The procedure combines a partial feedback linearization of the plant with a fixed-structure multi-model H_∞ design technique. Our methodology also includes a preliminary μ-based validation phase, during which worst-case models are obtained and then used to enrich the set of design models. Finally, a global nonlinear robustness analysis strategy is briefly sketched and the paper concludes with a detailed application of the methodology to a realistic aircraft landing problem. Future work will be devoted to further improvements of the design strategy and its application to a small autonomous aircraft, including flight tests ■

References

[1] J. ACKERMANN - *Multi-Model Approaches to Robust Control System Design*. Uncertainty and Control. Vol. 70 of Lecture Notes in Control and Information Sciences. Springer Berlin Heidelberg, p. 108-130, 1985.

[2] R. ADAMS, S. BANDA - *Robust Flight Control Design Using Dynamic Inversion and Structured Singular Value Synthesis.* IEEE Transactions on Control Systems Technology 1 (2), p. 80-92, 1993.

[3] P. APKARIAN, D. NOLL - *Non-Smooth H_∞ Synthesis*. IEEE Transactions on Automatic Control 51 (1), p. 71-86, 2006.

[4] J.-M. BIANNIC, L. BURLION, H. DE PLINVAL - *Robust Control Design Over Large Flight Envelopes: A Promising Approach for Aerial Robotics*. Issue 8 of the AerospaceLab Journal. http://www.aerospacelab-journal.org/aerial-robotics, 2014.

[5] J.-M. BIANNIC, L. BURLION, S. TARBOURIECH, G. GARCIA - *On Dynamic Inversion with Rate Limitations*. Proceedings of the American Control Conference. Montreal, QC, p. 191-196, 2012.

[6] Z. BING-YU, M. BLAISE - *Robustness Analysis of Dynamic Inversion Control Laws Applied to Nonlinear Aircraft Pitch-Axis Models*. Nonlinear Analysis Theory, Methods and applications 32 (4), p. 501-532, 1998.

[7] J.-L. BOIFFIER - *The Dynamics of Flight: The Equations*. Dynamics of Flight Series. Wiley, 1998.

[8] A. FRANCO, H. BOURLÈS, E. D. PIERI, H. GUILLARD - *Robust Nonlinear Control Associating Robust Feedback Linearization and H_∞ Control*. IEEE Transactions on Automatic Control 51 (7), p. 1200-1207, 2006.

[9] S. GUMUSSOY, M. OVERTON - *Fixed-Order H_∞ Controller Design via HIFOO, a Specialized Non-Smooth Optimization Package*. Proceedings of the American Control Conference. Seattle, USA, p. 2750-2754, 2008.

[10] A. ISIDORI - *Nonlinear Control Systems.* Vol. 1 of Communications and Control Engineering. Springer, 1995.

[11] M. KARA MOHAMED, A. LANZON - *Design and Control of Novel Tri-Rotor UAV.* Proceedings of the 2012 UKACC International Conference on Control. Cardiff, Wales, p. 304-309, 2012.

[12] M. KARA MOHAMED, A. LANZON - *Effect of Unmodelled Actuator Dynamics on Feedback Linearized Systems and a Two Stage Feedback Linearization Method*. Proceedings of the 52nd IEEE Conference on Decision and Control. Florence, Italy, p. 841-846, 2013.

[13] G. LOOYE, H.-D. JOOS - *Design of Autoland Controller Functions with Multi-Objective Optimization*. Journal of Guidance, Control and Dynamics 29 (2), p. 475-484, 2006.

[14] J.-F. MAGNI - *Linear Fractional Representation Toolbox for Use with Matlab.* Tech. rep., ONERA, report and software available at http://w3.onera.fr/smac/, 2006.

[15] A. MARCOS, G. BALAS - *Development of Linear-Parameter-Varying Models for Aircraft*. Journal of Guidance, Control and Dynamics 27 (2), p. 218-228, 2004.

[16] A. MEGRETSKI, A. RANTZER - *System Analysis via Integral Quadratic Constraints*. IEEE Transactions on Automatic Control 42 (6), p. 819-830, 1997.

[17] M. NEWLIN, P. YOUNG - *Mixed μ Problems and Branch and Bound Techniques*. International Journal of Robust and Nonlinear Control 7 (2), p. 145-164, February 1997.

[18] C. PAPAGEORGIOU, K. GLOVER -*Robustness Analysis of Nonlinear Dynamic Inversion Control Laws with Application to Flight Control.* Proceedings of the 43rd IEEE Conference on Decision and Control. Vol. 4. Nassau, The Bahamas, p. 3485-3490, 2004.

[19] C. PAPAGEORGIOU, K. GLOVER - *Robustness Analysis of Nonlinear Flight Controllers.* Journal of Guidance, Control and Dynamics 28 (4), p. 639-648, 2005.

[20] J. REINER, G. BALAS, W. GARRARD - *Robust Dynamic Inversion for Control of Highly Maneuverable Aircraft*. Journal of Guidance, Control and Dynamics 18 (1), p. 18-24, 1995.

[21] J. REINER, G. BALAS, W. GARRARD - *Flight Control Design Using Robust Dynamic Inversion and Time-Scale Separation.* Automatica 32 (11), p. 1493-1504, 1996.

[22] C. ROOS - *Systems Modeling, Analysis and Control (SMAC) Toolbox: An Insight into the Robustness Analysis Library.* Proceedings of the IEEE Multiconference on Systems and Control. Hyderabad, India, p. 176-181, 2013.

[23] C. Roos, G. Hardier, J.-M. Biannic - *Polynomial and Rational Approximation with the APRICOT Library of the SMAC Toolbox*. Proceedings of the IEEE Multiconference on Systems and Control. Antibes, France, 2014.

[24] C. ROOS, F. LESCHER, J.-M. BIANNIC, C. DOLL, G. FERRERES - *A Set of μ-Analysis Based Tools to Evaluate the Robustness Properties of High-Dimensional Uncertain Systems*. Proceedings of the IEEE Multiconference on Systems and Control. Denver, CO, USA, p. 644-649, 2011.

[25] S. A. SNELL, F. DALE, L. WILLIAM GARRARD - *Nonlinear Inversion Flight Control for a Supermaneuverable Aircraft.* Journal of Guidance, Control, and Dynamics 15 (4), p. 976-984, 1992.

[26] The MathWorks, Inc., 2014. *Robust Control Toolbox for Use with MATLAB.* Release 2014a. Natick, Massachusetts, United States., http://www.mathworks.com/help/robust/mu-synthesis.html.

Jean-Marc Biannic graduated from SUPAERO Engineering School in 1992 and received the PhD degree in Robust Control Theory with the highest honors in 1996 from SUPAERO as well. He joined ONERA as a research scientist in 1997 and received the HDR degree (French habilitation as PhD supervisor) from Paul Sabatier's University of Toulouse in 2010. Jean-Marc Biannic has supervised 6 PhD students. He is the author or co-author of 20 journal papers, beyond 50 conference papers, many book chapters, teaching documents, a tutorial book on multivariable control and Matlab toolboxes. He received in 2011 the second research distinction grade(MR2) from ONERA and the "ERE" distinction from ISAE (Aeronautics and Space Institute) thanks to which he is recognized as a full-professor in PhD committees. Jean-Marc Biannic has participated to several European projects and Garteur Groups (on PIO and nonlinear control). From 2012 to 2016, he has led a research project involving 10 research scientists for the development of the SMAC toolbox (w3.onera.fr/smac) for systems modeling, analysis and control.

Jérémy Lesprier is currently working as a professional engineer in the Attitude and Orbit Control Systems Development & Studies Department at Airbus Defence and Space, Toulouse, France. He graduated from the French engineering school *Arts et Métiers* ParisTech with a double degree in Aerospace Engineering at KTH (Stockholm, Sweden) in 2012. He received his Ph.D degree in automatic control from the University of Toulouse in 2015, for his work on robust control laws design, robustness analysis, and modeling for aerospace applications.

Clément Roos graduated from ISAE-SUPAERO in 2004 and holds a PhD in Automatic Control. He joined ONERA as a research scientist in 2007. He takes part in industrial projects with Airbus, Dassault and Safran. He is or was also involved in several European projects such as GARTEUR-AG17, COFCLUO, CLEANSKY, ERA and VISION. His research interests focus on aircraft modeling, robustness analysis and control laws validation, as well as robust and nonlinear control. He is the author or co-author of several papers, book chapters, teaching documents and Matlab tools implemented in the Systems Modeling, Analysis and Control toolbox.